

Article

Bifunctional Polymeric Carbon Nitride via Tuning Fabrication Conditions for Photocatalysis

Malgorzata Aleksandrzak ^{*} , Daria Baranowska, Wojciech Kukulka , Magdalena Onyszko, Beata Zielinska  and Ewa Mijowska 

Nanomaterials Physicochemistry Department, Faculty of Chemical Technology and Engineering, West Pomeranian University of Technology, Szczecin, Piastow Ave. 42, 71-065 Szczecin, Poland; bd36293@zut.edu.pl (D.B.); wojciech_kukulka@zut.edu.pl (W.K.); Magdalena.Onyszko@zut.edu.pl (M.O.); bzielinska@zut.edu.pl (B.Z.); emijowska@zut.edu.pl (E.M.)

* Correspondence: mwojtoniszak@zut.edu.pl; Tel.: +48-91-449-6031

Abstract: In this contribution, the hydrogen evolution reaction and photodegradation of Rhodamine B (RhB) dye were studied using urea-based polymeric carbon nitride (PCN) as photocatalyst. The effects of calcination temperature and heating rate of the PCN on structural, morphological, optical, photoelectrochemical, and photocatalytic properties were addressed. Different properties were found to be crucial in boosting photocatalytic performance depending on the reaction type. The highest efficiency in hydrogen evolution was observed in the presence of PCN characterized by the superior charge transport and charge lifetime properties arising from higher degree of structural arrangement and lower defect content in comparison to that of other photocatalysts. However, photocatalytic degradation of RhB was the most powerful when the catalyst exhibited the highest specific surface area as a key parameter determining its efficiency, although it presented lower charge transport and charge carrier properties.

Keywords: polymeric carbon nitride; photocatalysis; hydrogen; water splitting; RhB decomposition



Citation: Aleksandrzak, M.; Baranowska, D.; Kukulka, W.; Onyszko, M.; Zielinska, B.; Mijowska, E. Bifunctional Polymeric Carbon Nitride via Tuning Fabrication Conditions for Photocatalysis. *Catalysts* **2021**, *11*, 651. <https://doi.org/10.3390/catal11060651>

Academic Editors: Wonyong Choi, Detlef W. Bahnemann, Ioannis Konstantinou, Ewa Kowalska, Magdalena Janus, Vincenzo Vaiano and Zhi Jiang

Received: 25 February 2021

Accepted: 20 May 2021

Published: 21 May 2021

Publisher's Note: MDPI stays neutral with regard to jurisdictional claims in published maps and institutional affiliations.



Copyright: © 2021 by the authors. Licensee MDPI, Basel, Switzerland. This article is an open access article distributed under the terms and conditions of the Creative Commons Attribution (CC BY) license (<https://creativecommons.org/licenses/by/4.0/>).

1. Introduction

In recent years, polymeric carbon nitride received great interest since its discovery by Guy–Lussac in 1815 [1]. Next, a huge increase in interest in polymeric carbon nitride (PCN) was observed after the theoretical work of Liu and Cohen published in 1989 [2]; they believed that carbon nitrides were harder than diamonds. Several allotropes of carbon nitride such as alpha (α -C₃N₄), beta (β -C₃N₄), graphitic (g-C₃N₄, GCN), cubic, and pseudocubic C₃N₄ were predicted [3]. Among them, polymeric carbon nitride with 2D structures is regarded to be the most stable allotrope of carbon nitride at ambient conditions [4,5]. Moreover, PCN exhibits many remarkable physicochemical properties, including nontoxicity, high hardness, thermal, and chemical stability, a low friction coefficient, luminescence, inoxidizability, biological compatibility, and waterproofness [6,7]. These advantages stimulated much research into the use of PCN as a promising catalyst for many applications, including carbon dioxide activation, oxygen reduction, photocatalytic decomposition of organic pollutants, and photocatalytic hydrogen generation. Due to a suitable band gap in the visible light range (~2.7 eV) and outstanding physicochemical stability, PCN is intensively studied in photocatalytic processes [8]. However, PCN has disadvantages including structural disorder, low conductivity, low surface area, low effectiveness of electron-hole separation, poor dispersibility, and others that limit their utility. There are many strategies to improve the photocatalytic performance of PCN and one of them is the optimization of its synthesis route, which can tune catalytic performance [9]. Others might include preparation of bionanocomposites. Murugan et al. synthesized gCN@TiO₂ nanocomposite with different wt.% of gCN. They reported enhanced PEC

water splitting performance of nanocomposites compared to that of pure TiO₂ and gCN, which was due to the formation of heterojunction [10].

PCN can be synthesized by different approaches, such as thermal condensation, thermal nitridation, physical vapor deposition (PVD) [11], chemical vapor deposition (CVD) [12], solid-state reaction, and solvothermal method [13]. Among these methods, thermal pyrolysis is a relatively simple technique that does not require additives other than nitrogen-rich precursors. Depending on reaction conditions, the produced material exhibits different degrees of condensation, morphological properties, and reactivity. PCN synthesis via pyrolysis of urea at various temperatures was studied [1,14–16]. For example, D. R. Paul et al. [15] described the effect of calcination temperature (350–750 °C) on the properties of PCN. PCN obtained at 550 °C exhibited 12-times higher activity in comparison to that of the material synthesized at 450 °C. Authors argued that the high photoactivity is due to the appropriate degree of polymerization and condensation, enhancing light absorption abilities and a higher surface area resulting in better dye adsorption due to higher abundance of active sites. D. Das et al. [16] prepared PCN by pyrolysis of urea at four different temperatures: 350, 450, 550, and 650 °C. They stated that synthesis parameters tailor the number of defects or content of N–H functional groups present in the prepared materials. The presence of defects can change the lifetime of the carrier in the samples that, in turn, change PL (photoluminescence) properties and consequently their photocatalytic performance. J.H. Kim et al. [17] revealed that two parameters such as temperature and heating rate have the most significant influence on the structure and properties of PCN. When g-C₃N₄ is synthesized at a relatively high temperature, the amount of the obtained samples is reduced. However, the product exhibits optical properties typical for highly efficient photocatalyst via the increase in the thickness and defects formed in the PCN nanosheets. PCN also prepared via thermal pyrolysis of melamine (pyrolysis temperature: 500–700 °C; gas atmosphere: air, Ar, N₂) [18]. Air atmosphere dominantly favored a formation of layered PCN structure in comparison to that of those pyrolyzed in argon or nitrogen. The optimized PCN showed significant photodegradation, with a degradation rate of $4.4 \times 10^{-2} \text{ min}^{-1}$ of RhB removal under simulated solar radiation. A large surface area of $42 \text{ m}^2\text{g}^{-1}$ and suitable band energetics is attributed to better degradation performance.

The effects of the type of precursor and preparation conditions on the efficiency of PCN were also studied [3,19,20]. E. Alwin et al. [19] stated that the most efficient was the synthesis from dicyandiamide (~53%). Whereas the yield of pyrolysis process using melamine and thiourea as precursors were ~26 and ~11%, respectively. Besides, the general trends were described: (1) the yield of synthesis of carbon nitride decreases in the following order: melamine > dicyandiamide > thiourea > urea; (2) higher temperature decreases the production yield regardless of the precursor used; (3) the specific surface area is inversely proportional to the synthesis yield and increases in the following order: melamine < dicyandiamide < thiourea < urea; (4) higher synthesis temperature gives carbon nitrides with higher specific surface area, and (5) the reduction of the band gap of carbon nitrides obtained at higher temperature was observed. Moreover, Y. Zheng et al. [20] confirmed that the pyrolysis of urea given g-C₃N₄ with smaller crystalline domains and larger surface areas in comparison to melamine. They stated that used precursors and temperature of pyrolysis have a significant impact on the adsorption properties and photocatalytic activity of the obtained PCN. PCN produced from urea at a higher temperature (650 °C) exhibited the highest photocatalytic activity (9-times higher than that of g-C₃N₄ synthesized from melamine) in the Rhodamine B (RhB) decomposition under visible light irradiation ($\lambda > 410 \text{ nm}$).

The current state of the art presents several studies on structural and photocatalytic properties of PCN dependent on synthesis parameters. These papers report photocatalytic properties of PCN in hydrogen evolution reaction or dye degradation. However, none of them illustrated that different properties of a photocatalyst are crucial for the efficiency of the photocatalytic process dependent on the reaction type. In the present work, polymeric

carbon nitride was synthesized via direct pyrolysis of urea in the air atmosphere. The effect of preparation temperature (500–600 °C) and heating rate (1–5 °C/min) on composition, structure, and properties of PCN was investigated. Here, the analysis of morphology, texture, and optical properties tuning heating temperature and heating rate were attentively addressed. The activity of the synthesized samples was studied in the reaction of photocatalytic hydrogen generation using lactic acid as a sacrificial reactant under simulated solar light irradiation. Additionally, the photoactivity of PCN was evaluated in RhB decomposition under visible light.

2. Results and Discussion

2.1. Morphology and Structure

Atomic force microscopy was used to characterize topography and thickness of the prepared polymeric carbon nitrides. The analysis indicated that the formation temperature has moderate effect on the PCN sizes but significant effect on its thickness (Table 1). The representative AFM images and height profiles of the materials are presented in Figure S1 (see supplementary material).

Table 1. Flake size and thickness distribution of PCN prepared at 500, 520, 550, and 600 °C (500-4, 520-4, 550-4, and 600-4, respectively).

Sample	Size Range (mean, std. dev.)/nm	Thickness Range (mean, std. dev.)/nm
500-4	25–258 (43, 11.2)	1.8–13.3 (3.9, 1.4)
520-4	28–396 (49, 13.6)	1.5–12.4 (3.5, 1.2)
550-4	28–446 (48, 12.8)	1.2–8.5 (2.7, 0.8)
600-4	27–339 (50, 14.4)	0.8–13.6 (2.4, 0.9)

Transmission electron microscopy was further used to investigate a morphology of the prepared samples. Figure 1 presents transmission electron microscopy (TEM) images of PCN synthesized at 500, 520, 550, and 600 °C with a heating rate of 4 °C/min. Each sample shows a typical morphology of polymeric carbon nitride with tendency to wrinkle at the edges. In accordance to AFM analysis, the sizes of the flakes are comparable among the presented materials with the smallest nanosheets sizes of ~30 nm. No significant difference between the sample morphology is observed, although an increase in the calcination temperature affected increase in the transparency of the nanosheets.

X-ray diffraction (XRD) patterns were used to determine the crystal structure of PCN prepared under different conditions. Figure 2a shows typical XRD patterns of the polymeric carbon nitride. All the patterns contain diffraction peaks characteristic of carbon nitride, including peaks at around 13°, 27°, 44°, 57°, and 81°, which are related to the (100), (002), (200), (004), and (220) Bragg reflections, respectively (JCPDS: 01-087-1526). The observed lattice constants are $a = b = 4.7420 \text{ \AA}$ and $c = 6.7205 \text{ \AA}$, and this shows the hexagonal phase of PCN [21]. The strongest peak at around 27.3° represents the interplanar graphitic stacking of aromatic rings, and the peak at around 13.1° is indicative of in-planar structural packing motif of tri-s-triazine (heptazine) units in melon [22], demonstrating the formation of polymeric carbon nitride in the received samples [23]. Moreover, with increase in the calcination temperature, the (002) peak shifted to a higher angle (27.08° to 27.41°), depicting the corresponding change in the interlayer distance. This can be interpreted as an improved interlayer stacking order produced by the higher calcination temperature [24]. Besides, it can be clearly seen that the (002) peaks become more intense and narrower with increase in the calcination temperature, indicating more regular structure within the layers of PCN samples [14]. The (100) peak was found to be intense and narrow for all PCN samples, providing higher degree of polymerization [15]. Moreover, the (100) peak shifted to a smaller angle (13.07° to 12.70°) with a rise in calcination temperature, proving lowered long-range order of the in-plane structural packing in the PCN sheets [24]. Additionally, the different heating rates also had an impact on the position of the mentioned peaks. In

this case, the opposite relationship was observed. More specifically, (002) peak shifted to a smaller angle (27.58° to 27.26°), and (100) peak shifted to a higher angle (12.67° to 12.98°) with a rise in heating rate. This can be explained by the distortion of the tri-s-triazine unit (heptazine) due to the heating rate, which occurred in-plane instead of interplane.

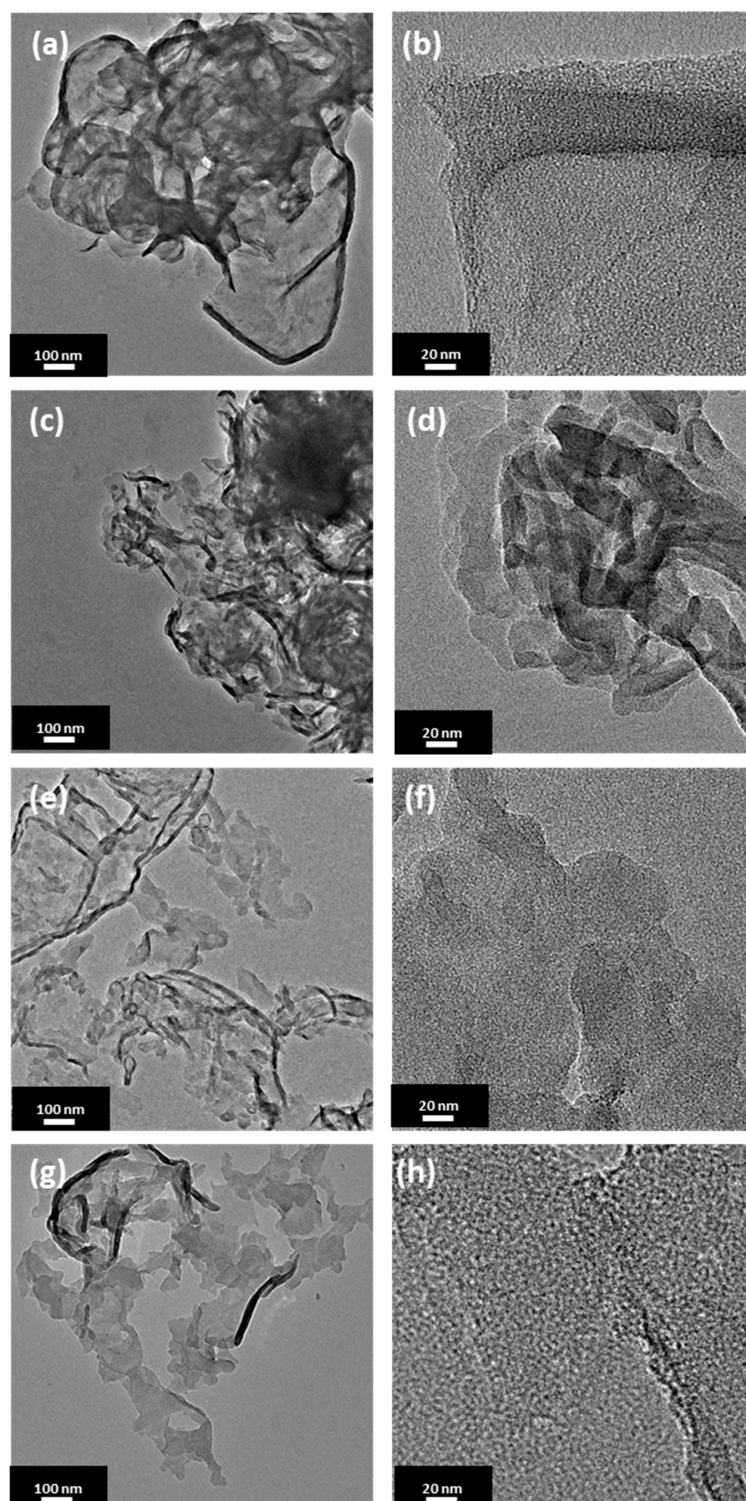


Figure 1. Transmission electron microscopy (TEM) images of polymeric carbon nitride prepared under different temperatures with $4^\circ\text{C}/\text{min.}$ of heating rate: (a,b) 500-4, (c,d) 520-4, (e,f) 550-4, and (g,h) 600-4.

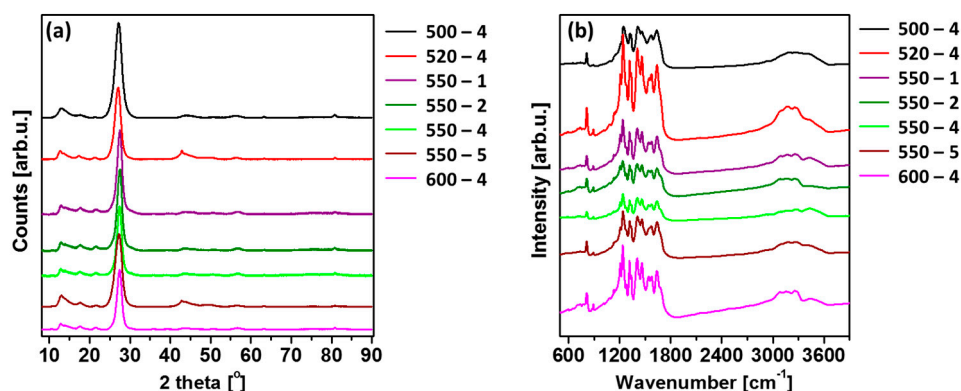


Figure 2. (a) X-ray diffraction (XRD) patterns; (b) Fourier transform infrared (FTIR) spectra of polymeric carbon nitride prepared under different conditions.

Fourier transform infrared (FTIR) spectra of as-prepared PCN samples are shown in Figure 2b. A strong peak observed at 815 cm^{-1} was designated to breathing mode of s-triazine units [25–28], which corresponds to condensed CN heterocycles. The bands observed at ~ 1650 , 1570 , 1410 , 1330 , and 1240 cm^{-1} are mainly assigned to the stretching vibrational mode of C=N. The modes from C–N heterocycles are in the range of $1200\text{--}1650\text{ cm}^{-1}$ [29–31]. The broad absorption band observed between 3000 and 3600 cm^{-1} was due to N–H stretching of amino groups and H_2O molecules absorbed on the samples [32–35]. Besides, the significant peak in the 550-2 sample appeared at 2900 cm^{-1} was attributed to the CH_2 vibrations. The presence of the CH_2 , N–H, and O–H band indicate the presence of the contamination of hydrogen and oxygen in the samples [36]. The FTIR patterns of the samples are in agreement with the results of XRD.

The chemical composition and relative atomic percentages of the obtained materials were analyzed by X-ray Photoelectron Spectroscopy (XPS) measurements. The XPS spectra showed that the obtained samples were mainly composed of carbon and nitrogen, but also had small amount of oxygen. Assuming a homogeneous distribution in the analyzed surface layer, the atomic concentration of these elements were calculated and given in Table 2. The obtained results show that nitrogen, carbon, and oxygen content is similar for all three samples and the changes are slight. The highest nitrogen content is in the samples with an intermediate synthesis temperature (i.e., 520 and 550). Oxygen content, in turn, is the highest in the samples fabricated at the highest synthesis temperature (i.e., 600). The detailed analysis of the chemical components of carbon and nitrogen was done by peak fitting procedure applied to the N 1s and C 1s spectra of the obtained samples. The results are shown in Figure S2 and in Table 3. The binding energy type as well as the relative contribution of each component to the total area under the peak were calculated. The spectra for both N 1s and C 1s of the samples present the typical shapes as well as the peak positions (~ 399 and $\sim 288\text{ eV}$ for N 1s and C 1s, respectively) [37]. The N 1s spectra present three main contributions related to C– N_3 (N_3C), N–C=N (N_2C), and N– H_x contributions, while the C 1s region show three contributions assigned to C–C, N–C=N and C– NH_x [38]. The sample obtained at the highest temperature is characterized by the highest content of C–C/C=C/ N_3C components and the lowest content of N– H_x among all obtained samples. The synthesis of PCN from urea results in obtaining different distribution of bonds in comparison with melamine-derived carbon nitride. Regardless of the precursor type, the most intense signals come from N_2C (N 1s) and N–C=N (C 1s). The difference between the polymeric carbon nitride types appears in the subsequent bindings. The second most intense signal for the materials obtained from melamine are N_3C (N 1s) and C–C/C=C (C 1s). Next, in the order are N– H_x and CN– H_x signals [38,39]. In the case of our urea-derived materials, the intensities of the second and third signals are the opposite. Too low a process temperature results in a structure with a surface containing many more N–C=N bonds and noticeably fewer C– NH_x and N_3C bonds. Increasing the process temperature

reverses this trend. In general, the spectra of the melamine materials show a very low oxygen content.

Table 2. C, N, O atomic concentration of polymeric carbon nitride (PCN) synthesized at 500, 520, 550, and 600 °C.

Sample	C (at.%)	N (at.%)	O (at.%)
500-4	36.58	63.23	0.18
520-4	33.9	65.92	0.18
550-4	34.11	65.79	0.1
600-4	36.31	63.19	0.5

Table 3. Chemical composition of 500-4, 520-4, 550-4, and 600-4 calculated from peak fitting procedure applied to N 1s and C 1s spectra of samples.

Sample	N–C=N	C–NH _x	C–C/C=C	N ₂ C	N–H _x	N ₃ C
500-4	77.00	16.41	6.58	87.73	9.69	2.59
520-4	67.02	24.43	8.55	85.68	9.91	4.41
550-4	71.31	22.00	6.69	86.27	9.15	4.58
600-4	63.76	24.96	11.29	87.96	7.22	4.82

The XPS analysis clearly indicates that an increase in the calcination temperature results in reduction of N–C=N and rising of C–NH_x and N₃C in the analyzed samples, which proves reduction of the structural arrangement of PCN and formation of higher amount of bulk defects. These observations are opposed to those presented by J. Xu et al. [14], which can be related to different heating rate and time of reaction.

To understand both the calcination temperature and heating rate effect towards the specific surface area of PCN samples synthesized under different conditions, the nitrogen adsorption-desorption isotherms together with their corresponding multipoint Brunauer–Emmett–Teller (BET) plots were conducted and presented in Figure 3 and Table 4, respectively. The porosity of the all obtained samples was tested by the N₂ adsorption-desorption experiment. The typical IV isotherms with H3 hysteresis loops are observed in the samples, which is typical of mesoporous materials like titanium dioxide nanofibers [40] or carbon nitride discussed in this article. With the initial increase in the heating temperature, the structural properties are improved, i.e., the specific surface area and the total pore volume increase what confirms previous observations [41]. However, from a certain temperature, these parameters deteriorate again. The highest surface area and total pore volume were obtained at 550 °C and 4 °C/min heating rate. At the same time, heating rate conditions have a significant impact on the specific surface area and total pore volume. The initial acceleration of the heating rate up to 4 °C/min improves the structural properties, but further increase to 5 °C/min results in deterioration of the parameters. Here, PCN heated at 4 °C/min was found to present the highest specific surface area and total pore volume. Generally, the larger surface area facilitated the adsorption of more contaminants on the surface of the catalysts and correspondingly provided more active sites, which both could significantly enhance the photocatalytic water splitting and organic dye degradation performance [14]. Hence, PCN 550-4 is expected to present the highest photocatalytic activity in the studied reactions.

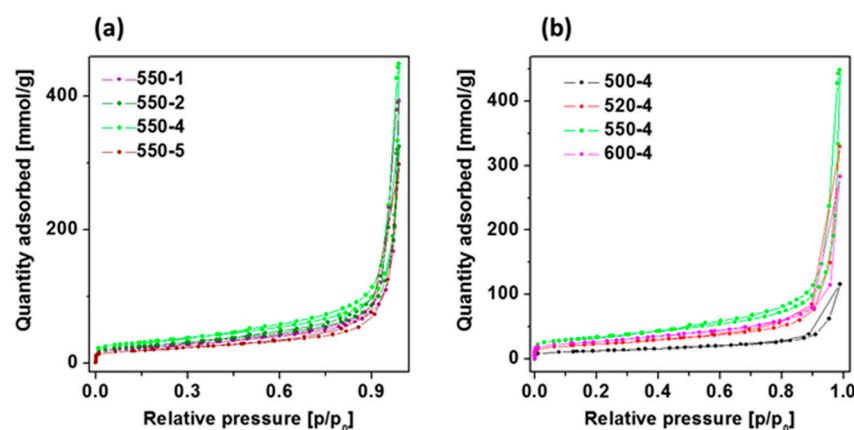


Figure 3. Adsorption-desorption isotherms of polymeric carbon nitride prepared at (a) 550 °C with different heating rate conditions and (b) under different temperatures (500–600 °C) with heating rate of 4 °C/min.

Table 4. Brunauer–Emmett–Teller (BET) surface area of polymeric carbon nitride prepared under different conditions.

Sample	550-1	550-2	550-4	550-5
BET surface area [m ² /g]	87.11 ± 0.09	96.98 ± 0.02	116.83 ± 0.10	72.49 ± 0.14
Total pore volume [cm ³ /g]	0.072	0.085	0.096	0.065
Sample	500-4	520-4	550-4	600-4
BET surface area [m ² /g]	44.83 ± 0.13	81.62 ± 0.07	116.83 ± 0.10	94.43 ± 0.01
Total pore volume [cm ³ /g]	0.034	0.069	0.096	0.083

2.2. Optical and Photoelectrical Properties

Diffuse reflectance spectra (DRS) spectra of polymeric carbon nitride prepared under different temperatures (500–600 °C) with heating rate of 4 °C/min were measured and presented in Figure 4a. Variation in the absorption edges was observed with the change in calcination temperature. The band gap energy of the samples, which were derived from the plots of the Kubelka–Munk function, obtained at 500, 520, 550, and 600 °C, were estimated to be 2.91, 2.89, 2.88, and 3.03 eV, respectively. To calculate values of E_g , the Tauc method was used, assuming the indirect band gaps of PCN were prepared at different conditions. When calcination temperature was raised from 500 to 520 and 550 °C, almost same value of E_g was observed. These slight differences could be due to the increased degree of polymerization of graphitic carbon nitride, resulting in an increase of π -plane conjugation degree of heptazine rings via N₂ atoms [14,42]. When the temperature was further raised to 600 °C, a band gap energy increased what can be a result of strong quantum confinement effect. This revealed that the band gap in the case of PCN prepared at 520 and 550 °C was narrower than samples prepared at 500 and 600 °C. It can be concluded that 520-4 and 550-4 had a higher ability to absorb visible light, which can lead to a better photoactivity in comparison to that of other samples [14,43].

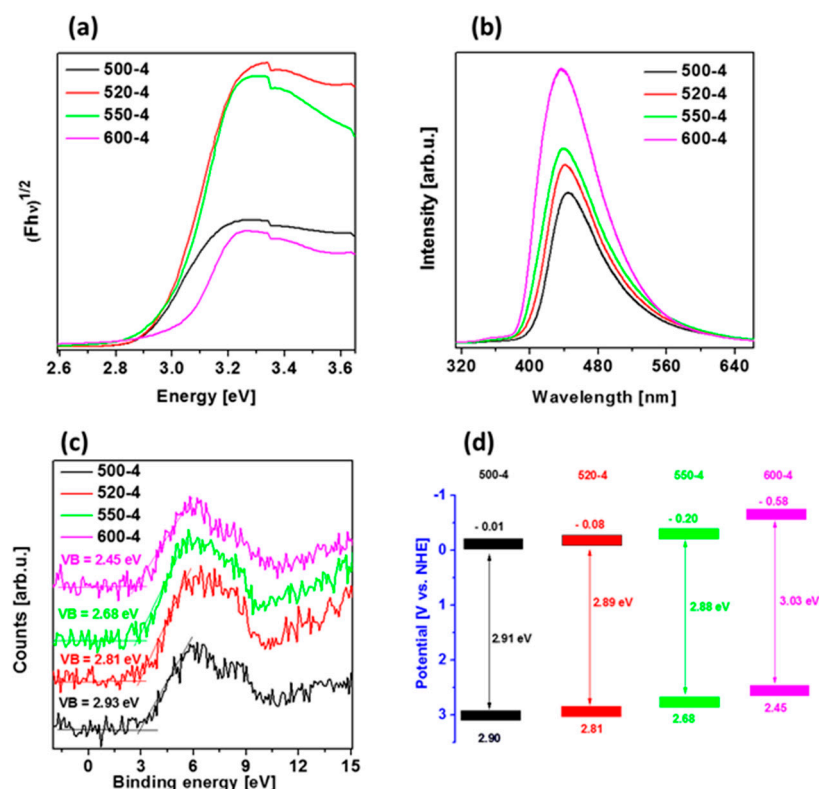


Figure 4. (a) Diffuse reflectance spectra (DRS) spectra, (b) photoluminescence (PL) spectra, (c) valence band (VB) X-ray Photoelectron Spectroscopy (XPS) spectra, and (d) band diagrams of polymeric carbon nitride prepared under different temperatures (500–600 °C) with heating rate of 4 °C/min.

The photoluminescence (PL) spectra of the samples were measured at room temperature with an excitation wavelength of 280 nm. As shown in Figure 4b, the 550-4 and 600-4 show a very strong emission peak centered at 439 nm, whose emission wavelength is shorter than that of 520-4 (440 nm) and 500-4 (445 nm). This effect is due to the enhanced condensation and packing between the layers caused by the increased temperature (from 500 to 600 °C), and the second observation is due to the quantum size effect [44–46], which can be verified by the fact that increasing calcination temperature leads to both, the gradual blue-shift of PL peak from 445 to 439 nm and increased PL intensity. These results indicate that the PL spectrum of polymeric carbon nitrides strongly depends on their structural defects and textural property.

To estimate valence band (VB) position of the materials, VB XPS spectra were measured and are presented in Figure 4c. Furthermore, conduction band position of the samples was calculated from the formula $E_{CB} = E_g - E_{VB}$, and band diagram is presented in Figure 4d. The VB and CB positions are shifted to the more positive potentials after temperature increase, indicating strengthened reducibility of the electrons in CB when one considers the hydrogen evolution reaction. The presented band diagrams of all materials indicate the possibility to create hydroxyl radicals because of more positive potentials of valence bands in comparison with that of $\text{OH}^- / \bullet\text{OH}$ potential (+1.99 eV vs. NHE). Simultaneously, only PCN prepared at 600 °C (600-4) is able to form superoxide radical, since its CB is more negative than $\text{O}_2 / \bullet\text{O}_2^-$ potential (−0.33 eV vs. NHE) [47]. However, this photocatalyst exhibits broad band gap (3.03 eV), indicating lower abilities for solar light harvesting.

For a deeper understanding of the transport behavior of the photogenerated charge carriers, transient photocurrent responses were employed under irradiation of 460, 532, 625, and 727 nm (Figure 5). It indicates the separation efficiency of the photogenerated charge carriers. The highest photocurrent response is achieved at 460 nm, which is consistent with the absorption band edge of polymeric carbon nitride prepared under different conditions.

The result indicates that the photocurrent response of PCN increased with the calcination temperature rising from 500 to 520 °C. Further increase in the preparation temperature to 550 and 600 °C leads to decreased photocurrent response. Comparing heating rate, the highest photocurrent response is established to the lowest heating rate value 550-1, which is 1.41 times higher than 550-4. Here, the measurements of photocurrent response under 460 nm irradiation are in agreement with the measurement under higher excitation wavelength.

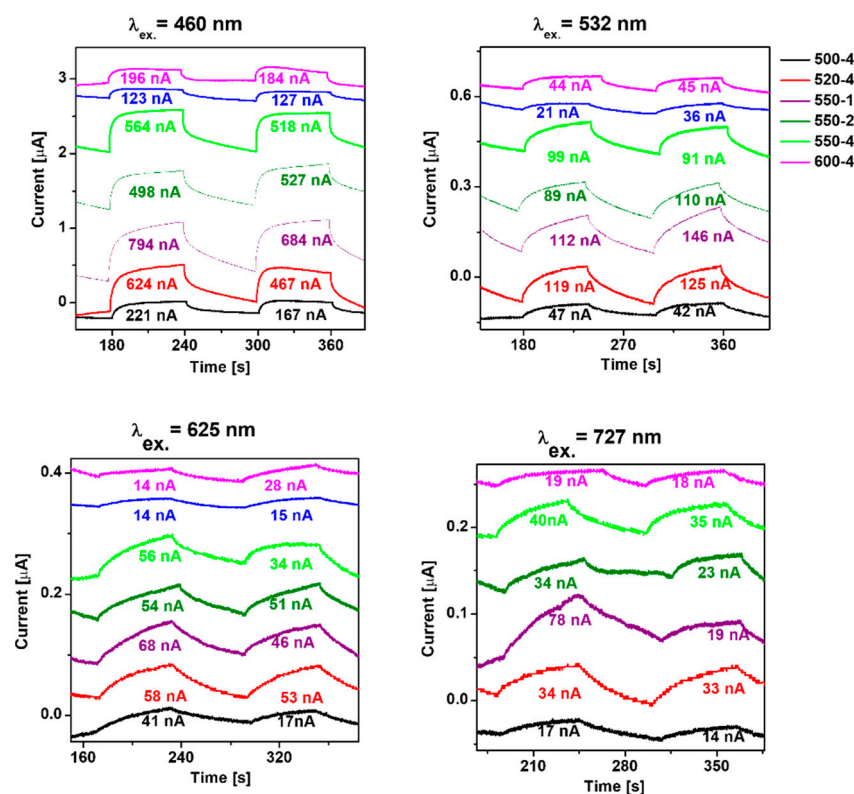


Figure 5. Photocurrent response of polymeric carbon nitride prepared under different conditions.

2.3. Photocatalytic Properties and their Relation to Structural and Physicochemical Properties of PCN

2.3.1. Hydrogen Evolution Reaction

The hydrogen evolution was carried out to study the effect of calcination conditions of urea (temperature and heating rate) on the photocatalytic performance of the obtained polymeric carbon nitride, which is presented in Figure 6a. Since lactic acid was used as electron donor (hole scavenger), O₂ is not produced during the photocatalytic reaction. Hence, the back reaction to produce water is suppressed, increasing the H₂ yield. Among all PCN samples prepared at 550 °C, the most efficient heating rate was established to be 4 °C/min, and it evolved ~5 μmol/g in 4 h. Hence, this heating rate value was further used to establish the optimal calcination temperature. Comparing the effect of calcination temperature, the maximum hydrogen evolution of ~9 μmol/g in 4 h is achieved at 520 °C—it is 1.7 times higher than 550-4. A histogram of H₂ evolution rate showing its dependence on preparation conditions is observed in Figure 6b, and the maximum hydrogen evolution rate of 2.12 μmol/gh is achieved in the 520-4 sample. The highest efficiency of polymeric carbon nitride prepared at 520 °C with heating rate of 4 °C/min is attributed to the most effective charge transport and separation properties, as it was revealed with chronoamperometry (Figure 5). It means that higher amount of photogenerated electrons could take part in photocatalytic reduction of protons to evolve hydrogen. The improved photocurrent response, and as a consequence, the highest photocatalytic activity, was a result of optimal structural properties. Although, the increase in calcination temperature

resulted in preparation of PCN with higher BET specific surface area and total pore volume, the higher content of bulk defects could probably act as recombination sites, which resulted in deterioration of the photocatalysis rate.

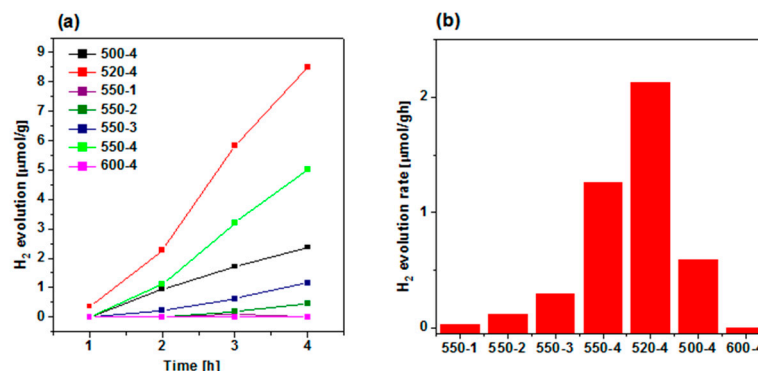
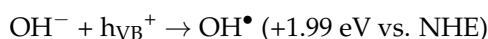


Figure 6. (a) Photocatalytic hydrogen evolution catalyzed by polymeric carbon nitride synthesized under different conditions. (b) H₂ evolution rates of catalysts. Reactions were performed under irradiation with Xe lamp (150 W) and air mass filter (A.M. 1.5 G) to achieve simulated solar light.

2.3.2. RhB Degradation Reaction

The photocatalytic activity of PCN synthesized under different conditions was examined in photocatalytic RhB decomposition under simulated solar light irradiation (Figure 7a). Additionally, blank test (organic dye decomposition without catalyst) and popular photocatalyst, TiO₂ (P25), was examined in the same conditions. The blank test confirms that RhB cannot be decomposed without use of catalyst. The photocatalytic ability of PCN is strongly related to the synthesis temperature. The efficiency of sample prepared at 500 °C is established to 55%, whenever all samples prepared at higher temperatures achieve at least twice times higher efficiency. Among them, the best results are reached for the samples prepared at 550 °C with different heating rates. Full degradation of organic dye is achieved for 550-2 sample after 5 h of simulated solar light illumination. Other PCN samples prepared at 550 °C exhibit slightly lower efficiency. Additionally, the UV/Vis spectra of RhB during degradation reaction with PCN 520-4 is shown in Figure S3. The photocatalytic degradation of RhB under simulated solar light irradiation follows the pseudo-first-order kinetics model (Figure 7b). Therefore, the rate constant k (1/min) of dye decomposition was estimated from the slope of $\ln(C/C_0) = -k \cdot t$ plots, where C_0 , C , and t are the initial dye concentration, the dye concentration at time t , and irradiation time, respectively [46,48]. Table 5 presents the photocatalytic dye decomposition kinetic parameters, such as pseudo-first-order rate constant and correlation coefficient. The estimated rate values of PCN prepared at 550 °C with different heating rates are higher than PCN prepared at other temperatures, indicating faster and more effective photocatalytic degradation of RhB as a model organic dye decomposition. The highest rate constant ($k = 0.55 \text{ min}^{-1}$) was established for PCN prepared at 550 °C with 4 °C/min heating rate, which is almost the same as for TiO₂ P25 ($k = 0.57 \text{ min}^{-1}$). The highest rate constant of RhB degradation in the presence of PCN 550-4 is attributed to the highest BET specific surface area. Although PCN prepared at 550 °C was characterized by inferior charge transport properties and shorter lifetime of charge carriers which was a result of higher defect content in comparison with PCN prepared at 520 °C, it presented higher BET surface area, which could play a key role in the acceleration of the reaction rate. Proposal mechanism of RhB decomposition in the presence of 550-4 is shown below:



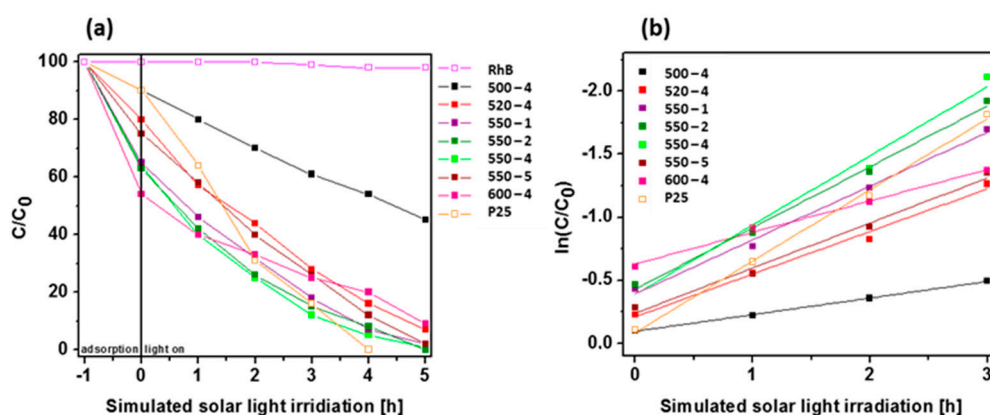
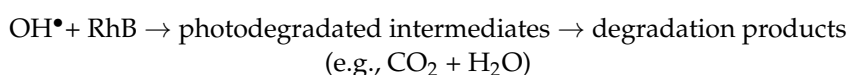


Figure 7. (a) Photodegradation of Rhodamine B (RhB) as a function of irradiation time over polymeric carbon nitride synthesized under different conditions. Reactions were performed under simulated solar light irradiation. (b) Relationship between RhB degradation efficiency and light irradiation time.

Table 5. Photocatalytic RhB decomposition kinetic parameters.

Sample	k [1/min]	R ²
500-4	0.13167	0.99878
520-4	0.33779	0.98535
550-1	0.42660	0.99197
550-2	0.48417	0.99289
550-4	0.54865	0.98117
550-5	0.35724	0.98510
600-4	0.24916	0.99161
P25	0.56510	0.99664

3. Materials and Methods

3.1. Synthesis of Polymeric Carbon Nitride

Polymeric carbon nitride was synthesized via heating of urea in air in an alumina crucible with a cover placed in a muffle furnace. Conditions of the preparation are listed in Table 6. Samples are named T-h, where T represents temperature of pyrolysis and h indicates heating rate; for instance, sample named as 500-4 represents PCN prepared at 500 °C with heating rate of 4 °C/min. Each sample was pyrolysed for 4 h.

Table 6. Preparation conditions of polymeric carbon nitride.

Sample	Heating Rate [°C/min]	Temperature [°C]	Time [h]
500-4	4	500	4
520-4	4	520	4
550-1	1	550	4
550-2	2	550	4
550-3	3	550	4
550-4	4	550	4
550-5	5	550	4
600-4	4	600	4

3.2. Characterization

Morphology of the samples was analyzed using TEM (Tecnai F30) with 200 kV accelerating voltage. Topography and thickness of the materials were analyzed with atomic force microscopy (Nanoscope V MultiMode 8). XRD patterns were recorded on Empyrean

(Aeris, Malvern Panalytical) X-ray diffractometer. FTIR spectra were recorded on Nicolet 6700 FT-IR Spectrometer. BET-specific surface area and pore volume were measured by nitrogen sorption in the temperature of liquid nitrogen using a Micromeritics ASAP 2460. The pore size distribution of each sample was calculated using nonlocal density functional theory (NLDFT) from the desorption branch of the isotherms. The chemical composition and relative atomic percentages on the surface of the samples were studied by XPS. The measurements were conducted using Mg Ka ($h\nu = 1253.6$ eV) radiation in a Prevac (Poland) system equipped with a Scienta SES 2002 (Sweden) electron energy analyzer operating with constant transmission energy ($E_p = 50$ eV). The analysis chamber was evacuated to a pressure below $5 \cdot 10^{-9}$ mbar. The PL spectra were measured using fluorescence spectrophotometer F7000 (Hitachi) with excitation wavelength of 280 nm. The UV-vis DRS were performed using a Jasco (Japan) spectrometer. Kubelka–Munk function was used to calculate the band gap energy. Photocurrent response was measured on Autolab PGSTAT302 N potentiostat in a 3-electrode test cell with a platinum wire as counter electrode and saturated calomel electrode as reference. The working electrode was FTO glass with the analyzed material drop-casted from 0.2 % ethanol/nafion solution. 0.5 M sodium sulfate was used as the electrolyte. Photocurrent (chronoamperometry) test was measured at 0.5 V vs SCE.

3.3. Photocatalytic Reactions

Photocatalytic hydrogen evolution was conducted in an outer irradiation-type reactor connected to argon. 10 mg of a photocatalyst was dispersed in 20 mL of water and 2 mL of lactic acid at pH = 1.77 (at 21 °C). Prior to the photocatalytic reaction, the reactor was purged with argon for air removal. Afterwards, the suspension was illuminated with Xe lamp (150 W) with air mass filter (A.M. 1.5 G) to achieve a simulated solar light. The photocatalytic H₂ evolution rate was analyzed by Young Lin 6500 gas chromatograph (GC, Micro TCD detector, ValcoPLOT Molesieve 5 Å Fused Silica Column and Ar as a carrier).

The photocatalytic performance of the obtained samples was evaluate RhB decomposition under simulated solar light irradiation (halogen 150 W lamp with cutoff light filters of natural solar conditions, Photon Institute, Poland). Typically, for the reaction carried out under visible light irradiation, 50 mg of the catalyst was dispersed into 100 mL of aqueous RhB solution (5 mg/dm³) at pH = 6.25 (at 21 °C) in a cylindrical inner-irradiation-type quartz glass reactor. Visible-light irradiation was proceeded by stirring of the sample in darkness for 1 h to establish the adsorption-desorption equilibrium. Next, the mixture was irradiated for 5 h. 3 mL of the solution was used at equal time intervals and the absorbance was determined by UV-vis spectrophotometer (JASCO V-770). The decomposition efficiency of RhB was calculated according to the following equation: C/C_0 where C_0 and C stand for the initial concentration of dye solution and concentration after a predetermined irradiation time t .

4. Conclusions

In summary, polymeric carbon nitride prepared under different conditions was successfully synthesized and used as photocatalyst for hydrogen evolution reaction from water splitting and RhB decomposition. We found that both the heating rate and calcination temperature affected photocatalytic efficiency. These results confirm that the photocatalytic efficiency of polymeric carbon nitride strongly depend on its structural defects and textural properties. Moreover, different structural parameters influenced a photocatalytic performance in different types of reactions. More specifically, charge transport and charge lifetime properties arising from structural arrangement and defect content in PCN were found to determine the catalyst with the highest efficiency in hydrogen generation. However, the highest specific surface area was crucial for the second photocatalytic reaction: RhB degradation.

Supplementary Materials: The following are available online at <https://www.mdpi.com/article/10.3390/catal11060651/s1>, Figure S1: AFM images and height profiles of polymeric carbon nitride

prepared under different conditions: (a) 500-4, (b) 520-4, (c) 550-4 and (d) 600-4. Figure S2. C 1s and N 1s XPS spectra of polymeric carbon nitride synthesized at 500 °C (500-4) (a,b), 520 °C (520-4) (c,d), 550 °C (550-4) (e,f) and 600 °C (600-4) (g,h). Figure S3. UV/vis spectra of RhB during photocatalytic degradation with catalyst 520-4 irradiated with simulated solar light (150 W Xe lamp with Air Mass 1.5G filter).

Author Contributions: Conceptualization: M.A. and M.O.; methodology: M.A.; formal analysis: M.A., D.B., M.O. and W.K.; investigation: M.A., D.B., M.O. and W.K.; resources, M.A.; data curation, M.A.; writing—original draft preparation: M.A., D.B., W.K. and B.Z.; writing—review and editing, M.A. and E.M.; supervision, M.A. and E.M. All authors have read and agreed to the published version of the manuscript.

Funding: This research was funded by National Science Center, Poland, under SONATA program (no. 2015/19/D/ST5/01920).

Data Availability Statement: The data presented in this study are available online.

Conflicts of Interest: The authors declare no conflict of interest.

References

1. Thomas, A.; Fischer, A.; Goettmann, F.; Antonietti, M.; Müller, J.-O.; Schlögl, R.; Carlsson, J.M. Graphitic carbon nitride materials: Variation of structure and morphology and their use as metal-free catalysts. *J. Mater. Chem.* **2008**, *18*, 4893–4908. [[CrossRef](#)]
2. Liu, A.Y.; Cohen, M.L. Prediction of new low compressibility solids. *Science* **1989**, *245*, 841–842. [[CrossRef](#)]
3. Yew, Y.T.; Lim, C.S.; Eng, A.Y.S.; Oh, J.; Park, S.; Pumera, M. Electrochemistry of layered graphitic carbon nitride synthesised from various precursors: Searching for catalytic effects. *ChemPhysChem* **2016**, *17*, 481–488. [[CrossRef](#)]
4. Gracia, J.; Kroll, P. Corrugated layered heptazine-based carbon nitride: The lowest energy modifications of C₃N₄ ground state. *J. Mater. Chem.* **2009**, *19*, 3013–3019. [[CrossRef](#)]
5. Zheng, Y.; Liu, J.; Liang, J.; Jaroniec, M.; Qiao, S.Z. Graphitic carbon nitride materials: Controllable synthesis and applications in fuel cells and photocatalysis. *Energy Environ. Sci.* **2012**, *5*, 6717–6731. [[CrossRef](#)]
6. Dai, X.; Han, Z.; Fan, H.; Ai, S. Sulfur doped carbon nitride quantum dots with efficient fluorescent property and their application for bioimaging. *J. Nanoparticle Res.* **2018**, *20*, 315. [[CrossRef](#)]
7. Barrio, J.; Volokh, M.; Shalom, M. Polymeric carbon nitrides and related metal-free materials for energy and environmental applications. *J. Mater. Chem. A* **2020**, *8*, 11075–11116. [[CrossRef](#)]
8. Reddy, K.; Reddy, C.; Nadagouda, M.; Shetti, N.; Joesool, S.; Aminabhavi, T. Polymeric graphitic carbon nitride (g-C₃N₄)-based semiconducting nanostructured materials: Synthesis methods, properties and photocatalytic applications. *J. Environ. Manage.* **2019**, *238*, 25–40. [[CrossRef](#)] [[PubMed](#)]
9. Wang, Z.; Hu, X.; Zou, G.; Huang, Z.; Tang, Z.; Liu, Q.; Hu, G.; Geng, D. Advances in constructing polymeric carbon-nitride-based nanocomposites and their applications in energy chemistry. *Sustain. Energy Fuels* **2019**, *3*, 611–655. [[CrossRef](#)]
10. Murugan, C.; Bhojanaa, K.B.; Ong, W.J.; Jothivenkatachalam, K.; Pandikumar, A. Improving hole mobility with the heterojunction of graphitic carbon nitride and titanium dioxide via soft template process in photoelectrocatalytic water splitting. *Int. J. Hydrog. Energy* **2019**, *44*, 30885–30898. [[CrossRef](#)]
11. Gago, R.; Jiménez, I.; Caceres, D.; Agulló-Rueda, F.; Sajavaara, T.; Albella, J.M.; Climent-Font, A.; Vergara, I.; Räisänen, J.; Rauhala, E.; et al. Hardening mechanisms in graphitic carbon nitride films grown with N₂/Ar ion assistance. *Chem. Mater.* **2001**, *13*, 129–135. [[CrossRef](#)]
12. Chamorro-Posada, P.; Dante, R.C.; Vázquez-Cabo, J.; Dante, D.G.; Martín-Ramos, P.; Rubiños-López, Ó.; Sánchez-Arévalo, F.M. Experimental and theoretical investigations on a CVD grown thin film of polymeric carbon nitride and its structure. *Diam. Relat. Mater.* **2021**, *111*, 108169. [[CrossRef](#)]
13. Lu, D.; Fang, P.; Wu, W.; Ding, J.; Jiang, L.; Zhao, X.; Li, C.; Yang, M.; Li, Y.; Wang, D. Solvothermal-assisted synthesis of self-assembling TiO₂ nanorods on large graphitic carbon nitride sheets with their anti-recombination in the photocatalytic removal of Cr(vi) and rhodamine B under visible light irradiation. *Nanoscale* **2017**, *9*, 3231–3245. [[CrossRef](#)]
14. Xu, J.; Li, Y.; Peng, S.; Lu, G.; Li, S. Eosin Y-sensitized graphitic carbon nitride fabricated by heating urea for visible light photocatalytic hydrogen evolution: The effect of the pyrolysis temperature of urea. *Phys. Chem. Chem. Phys.* **2013**, *15*, 7657–7665. [[CrossRef](#)]
15. Paul, D.R.; Sharma, R.; Nehra, S.P.; Sharma, A. Effect of calcination temperature, pH and catalyst loading on photodegradation efficiency of urea derived graphitic carbon nitride towards methylene blue dye solution. *RSC Adv.* **2019**, *9*, 15381–15391. [[CrossRef](#)]
16. Das, D.; Banerjee, D.; Das, B.; Das, N.; Chattopadhyay, K. Effect of cobalt doping into graphitic carbon nitride on photo induced removal of dye from water. *Mater. Res. Bull.* **2017**, *89*, 170–179. [[CrossRef](#)]
17. Kim, J.H.; Ji, M.; Ryu, C.H.; Lee, Y.I. Effect of pyrolysis conditions on the physicochemical properties of graphitic carbon nitride for visible-light-driven photocatalytic degradation. *Arch. Metall. Mater.* **2020**, *65*.

18. Madhurima, V.; Borse, P.H.; Kumari, K.; Rao, T.; Jain, P. Improved photocatalytic activity of carbon-based polymeric semiconductor for efficient decontamination of wastewater: Effect of reaction atmosphere and pyrolysis temperature. *Opt. Mater.* **2020**, *110*, 110523. [[CrossRef](#)]
19. Alwin, E.; Kočí, K.; Wojcieszak, R.; Zieliński, M.; Edelmánová, M.; Pietrowski, M. Influence of high temperature synthesis on the structure of graphitic carbon nitride and its hydrogen generation ability. *Materials* **2020**, *13*, 2756. [[CrossRef](#)] [[PubMed](#)]
20. Zheng, Y.; Zhang, Z.; Li, C. A comparison of graphitic carbon nitrides synthesized from different precursors through pyrolysis. *J. Photochem. Photobiol. A Chem.* **2017**, *332*, 32–44. [[CrossRef](#)]
21. Nabi, G.; Malik, N.; Tahir, M.B.; Raza, W.; Rizwan, M.; Maraj, M.; Siddiq, A.; Ahmed, R.; Tanveer, M. Synthesis of graphitic carbon nitride and industrial applications as tensile strength reinforcement agent in red Acrylonitrile-Butadiene-Styrene (ABS). *Phys. B Condens. Matter* **2021**, *602*, 412556. [[CrossRef](#)]
22. Zhang, Y.; Liu, J.; Wu, G.; Chen, W. Porous graphitic carbon nitride synthesized via direct polymerization of urea for efficient sunlight-driven photocatalytic hydrogen production. *Nanoscale* **2012**, *4*, 5300–5303. [[CrossRef](#)] [[PubMed](#)]
23. Su, Q.; Sun, J.; Wang, J.; Yang, Z.; Cheng, W.; Zhang, S. Urea-derived graphitic carbon nitride as an efficient heterogeneous catalyst for CO₂ conversion into cyclic carbonates. *Catal. Sci. Technol.* **2014**, *4*, 1556–1562. [[CrossRef](#)]
24. Niu, P.; Liu, G.; Cheng, H.-M. Nitrogen vacancy-promoted photocatalytic activity of graphitic carbon nitride. *J. Phys. Chem. C* **2012**, *116*, 11013–11018. [[CrossRef](#)]
25. Xiang, Q.; Yu, J.; Jaroniec, M. Preparation and enhanced visible-light photocatalytic H₂-production activity of graphene/C₃N₄ composites. *J. Phys. Chem. C* **2011**, *115*, 7355–7363. [[CrossRef](#)]
26. Papailias, I.; Giannakopoulou, T.; Todorova, N.; Demotikali, D.; Vaimakis, T.; Trapalis, C. Effect of processing temperature on structure and photocatalytic properties of g-C₃N₄. *Appl. Surf. Sci.* **2015**, *358*, 278–286. [[CrossRef](#)]
27. Dong, F.; Wu, L.; Sun, Y.; Fu, M.; Wu, Z.; Lee, S.C. Efficient synthesis of polymeric g-C₃N₄ layered materials as novel efficient visible light driven photocatalysts. *J. Mater. Chem.* **2011**, *21*, 15171–15174. [[CrossRef](#)]
28. Liu, J.; Zhang, T.; Wang, Z.; Dawson, G.; Chen, W. Simple pyrolysis of urea into graphitic carbon nitride with recyclable adsorption and photocatalytic activity. *J. Mater. Chem.* **2011**, *21*, 14398–14401. [[CrossRef](#)]
29. Li, Y.; Lv, K.; Ho, W.; Zhao, Z.; Huang, Y. Enhanced visible-light photo-oxidation of nitric oxide using bismuth-coupled graphitic carbon nitride composite heterostructures. *Chin. J. Catal.* **2017**, *38*, 321–329.
30. Mo, Z.; She, X.; Li, Y.; Liu, L.; Huang, L.; Chen, Z.; Zhang, Q.; Xu, H.; Li, H. Synthesis of g-C₃N₄ at different temperatures for superior visible/UV photocatalytic performance and photoelectrochemical sensing of MB solution. *RSC Adv.* **2015**, *5*, 101552–101562. [[CrossRef](#)]
31. Martin, D.T.; Qiu, K.; Shevlin, S.A.; Handoko, A.D.; Chen, X.; Guo, Z.; Tang, J. Highly efficient photocatalytic H₂ evolution 526 from water light and structure controlled graphitic carbon nitride using visible. *Angew. Chem. Int. Ed.* **2014**, *126*, 9394–9399. [[CrossRef](#)]
32. Zimmerman, J.L.; Williams, R.; Khabashesku, A.V.N.; Margrave, J.L. Synthesis of spherical carbon nitride nanostructures. *Nano Lett.* **2001**, *1*, 731–734. [[CrossRef](#)]
33. Wang, Y.; Qiao, M.; Lv, J.; Xu, G.; Zheng, Z.; Zhang, X.; Wu, Y. g-C₃N₄/g-C₃N₄ isotype heterojunction as an efficient platform for direct photodegradation of antibiotic. *Fullerenes Nanotub. Carbon Nanostruct.* **2018**, *26*, 210–217.
34. Feng, W.; Fang, J.; Zhou, G.; Zhang, L.; Lu, S.; Wu, S.; Chen, Y.; Ling, Y.; Fang, Z. Rationally designed Bi@BiOCl/g-C₃N₄ heterostructure with exceptional solar-driven photocatalytic activity. *Mol. Catal.* **2017**, *434*, 69–79. [[CrossRef](#)]
35. Sucasaire, W.; Matsuoka, M.; Lopes, K.C.; Mittani, J.C.R.; Avanci, L.H.; Chubaci, J.F.D.; Added, N.; Trava, V.; Corat, E.J. Raman and infrared spectroscopy studies of carbon nitride films prepared on Si (100) substrates by ion beam assisted deposition. *J. Braz. Chem. Soc.* **2006**, *17*, 1163–1169. [[CrossRef](#)]
36. Lan, Y.; Li, Z.; Li, D.; Yan, G.; Yang, Z.; Guo, S. Graphitic carbon nitride synthesized at different temperatures for enhanced visible-light photodegradation of 2-naphthol. *Appl. Surf. Sci.* **2019**, *467*, 411–422. [[CrossRef](#)]
37. Dementjev, A.; de Graaf, A.; van de Sanden, M.; Maslakov, K.; Naumkin, A.; Serov, A. X-Ray photoelectron spectroscopy reference data for identification of the C₃N₄ phase in carbon–nitrogen films. *Diam. Relat. Mater.* **2000**, *9*, 1904–1907. [[CrossRef](#)]
38. Caudillo-Flores, U.; Rodriguez-Padron, D.; Muñoz-Batista, M.J.; Kubacka, A.; Luque, R.; Fernández-García, M. Facile synthesis of B/g-C₃N₄ composite materials for the continuous-flow selective photo-production of acetone. *Green Chem.* **2020**, *22*, 4975–4984. [[CrossRef](#)]
39. Tan, L.; Xu, J.; Zhang, X.; Jia, Y.; Wang, S. Synthesis of g-C₃N₄/CeO₂ nanocomposites with improved catalytic activity on the thermal decomposition of ammonium perchlorate. *Appl. Surf. Sci.* **2015**, *356*, 447–453. [[CrossRef](#)]
40. Ghosh, M.; Lohrasbi, M.; Chuang, S.S.C.; Jana, S.C. Mesoporous titanium dioxide nanofibers with a significantly enhanced photocatalytic activity. *ChemCatChem* **2016**, *8*, 2525–2535. [[CrossRef](#)]
41. Sun, S.; Liang, S. Recent advances in functional mesoporous graphitic carbon nitride (mpg-C₃N₄) polymers. *Nanoscale* **2017**, *9*, 10544–10578. [[CrossRef](#)]
42. Zhang, G.; Zhang, J.; Zhang, M.; Wang, X. Polycondensation of thiourea into carbon nitride semiconductors as visible light photocatalysts. *J. Mater. Chem.* **2012**, *22*, 8083–8091. [[CrossRef](#)]
43. Gu, Q.; Gao, Z.; Zhao, H.; Lou, Z.; Liao, Y.; Xue, C. Temperature-controlled morphology evolution of graphitic carbon nitride nanostructures and their photocatalytic activities under visible light. *RSC Adv.* **2015**, *5*, 49317–49325. [[CrossRef](#)]

44. Zhang, X.; Xie, X.; Wang, H.; Zhang, J.; Pan, B.; Xie, Y. Enhanced photoresponsive ultrathin graphitic-phase C₃N₄ nanosheets for bioimaging. *J. Am. Chem. Soc.* **2013**, *135*, 18–21. [[CrossRef](#)] [[PubMed](#)]
45. Wang, Y.; Wang, X.; Antonietti, M. Polymeric Graphitic Carbon Nitride as a Heterogeneous Organocatalyst: From Photochemistry to Multipurpose Catalysis to Sustainable Chemistry. *Angew. Chem. Int. Ed.* **2012**, *51*, 68–89. [[CrossRef](#)] [[PubMed](#)]
46. Wu, H.; Wu, X.-L.; Wang, Z.-M.; Aoki, H.; Kutsuna, S.; Jimura, K.; Hayashi, S. Anchoring titanium dioxide on carbon spheres for high-performance visible light photocatalysis. *Appl. Catal. B Environ.* **2017**, *207*, 255–266. [[CrossRef](#)]
47. Baca, M.; Aleksandrak, M.; Mijowska, E.; Kaleńczuk, R.J.; Zielińska, B. Core/shell structure of mesoporous carbon spheres and g-C₃N₄ for Acid Red 18 decolorization. *Catalysts* **2019**, *9*, 1007. [[CrossRef](#)]
48. Da Silva, C.G.; Faria, J.L. Photochemical and photocatalytic degradation of an azo dye in aqueous solution by UV irradiation. *J. Photochem. Photobiol. A Chem.* **2003**, *155*, 133–143. [[CrossRef](#)]